Chapter 5

Analytical Estimates of Bias and Variance in Presence of Time-Correlated Residual Gains *

In this chapter, we include the thermal noise and use error propagation to find analytical expressions for the bias and variance of the power spectrum in the presence of bright foreground, residual gain errors, and noise. We compare and validate the analytical estimates with simulated observations and use the former to investigate various effects of the gain errors in power spectrum estimation. We provide a method to calculate the best possible estimate for the 21-cm power spectrum for a given interferometer and discuss the measures to be taken to enhance the chance of detecting the 21-cm signal. Though some of the concepts were discussed in Chapter 4 already, we restate them here to maintain clarity.

*The content in this chapter is originally presented in Kumar et al. (2022)

5.1 Gain Error Model

In radio interferometric observations, a pair of antennas at a given time records the visibility function with modification by gains from different sources, including the gain of an individual antenna. The recorded signal includes measurement noise $\tilde{N}_i(\vec{U}_i)$. If a pair of antennas at a given time defines the baseline $\vec{U}_i(t)$, we may write the recorded visibility $\tilde{V}(\vec{U}_i)$ at this baseline in terms of noise and gains as (Hamaker et al., 1996; Taylor et al., 1999)

$$\tilde{V}(\vec{U}_i) = \tilde{G}_i(t)\tilde{V}_i^S(\vec{U}_i) + \tilde{N}_i(\vec{U}_i), \tag{5.1}$$

where $\tilde{G}_i(t)$ is the gain for the i^{th} baseline. Note that, for a given pair of antennas, the projected antenna separation and hence the baseline vector changes with time as the antenna follows the source position in the sky. Interferometric noise $\tilde{N}_i(\vec{U}_i)$ can be considered Gaussian random with zero mean. Given antenna characteristics and its source equivalent flux density (SEFD), frequency width of the channel $\Delta\nu$ and integration time for each visibility $\Delta\tau$, the standard deviation of the noise in the real or imaginary part of each visibility can be written as (Thompson et al., 1986)

$$\sigma_N(\vec{U}) = \frac{\text{SEFD}}{\sqrt{2\Delta\nu\,\Delta\tau}}. \tag{5.2}$$

It is safe to assume that the interferometric noise is uncorrelated in time. Hence, its auto-correlation functions are zero except at zero delay. Also, the sky signal, antenna gains, and noise have no cross-correlations.

The gain $\tilde{G}_i(t)$ in each visibility arises from the individual gains of the antenna pairs used to estimate it. If the ith measurement of visibility at a time t involves two antennae say A and B, then the gain $\tilde{G}_i(t)$ can be written as

$$\tilde{G}_i(t) = \langle \tilde{g}_A(t)\tilde{g}_B^*(t)\rangle, \tag{5.3}$$

where $\tilde{g}_A$ and $\tilde{g}_B$ are the gains of the individual antenna and the angle brackets represent the average over the integration time.

The first step to preparing the observed data for scientific purposes is to estimate the antenna gains using primary calibration or self-calibration methods. In the simulation, under perfect calibration, all gains are unity. In practice, interferometric calibration is affected by the non-zero noise in the system, the time-dependent ionospheric variation, the calibration algorithm used, etc. Here we assume that the best calibration procedure for the data in consideration has been applied, and only residual gains for each antenna contribute to the gain term $\tilde{G}_i(t)$. In such a case, we can write the gain from an individual antenna (say antenna A) as

$$\tilde{g}_A(t) = [1 + \delta_{AR}(t) + i\delta_{AI}(t)] \tag{5.4}$$

where $\delta_{AR}(t)$ and $\delta_{AI}(t)$ stands for the real and imaginary part of the residual gain error. As the best possible calibration is already performed, we assume the residual gains are small compared to unity and zero mean random numbers. Here we do not consider any frequency dependence of the gain and its polarisation properties. This work assumes the residual gain errors are Gaussian random and quantifies them with their variance and two-point correlation functions [†]. We further assume that the real and imaginary parts of the gain from a given antenna and residual gains from the different antennae are not correlated. These assumptions work fairly well in a real observation; however, there can be departure coming from unidentified low-level radio frequency interference, correlated structural change of the antenna with elevation, etc. All these effects change with observatories. These effects can be included in the framework we discuss here if needed. We denote the variance σ^2_{AC} and the normalized two-point correlation $\xi_{AC}(\tau)$ of the residual gain from antenna A as

$$\sigma^2_{AC} = \langle \delta^2_{AC} \rangle, \quad \xi_{AC}(\tau) = \langle \delta_{AC}(t)\delta_{AC}(t+\tau) \rangle / \sigma^2_{AC}, \tag{5.5}$$

[†]Note that the residual gain errors may have non-zero higher-order correlations and hence can have non-Gaussian properties. However, we expect the two-point correlations to dominate here.

where C is to be read as R or I for real and imaginary parts of the gain, and hence δ_{AC} can be δ_{AR} or δ_{AI} for the real or imaginary part of the gain respectively. The two-point correlation of the residual gains is a function of (time) delay τ and is normalized such that its value is unity at zero delay. Given an observation, it is possible to estimate these properties of the gain from the calibration solutions. Here, for simplicity, we assume that the statistical properties of the gains for all the antennas in the array are the same. We shall denote these as σ_R^2 and σ_I^2. We further assume that the normalized two-point correlation functions for all antennae are the same irrespective of them being of real or imaginary parts; we denote this by $\xi(\tau)$. The two-point correlation of the gain is expected to have contributions from various sources, including sky model errors, temperature fluctuations, instrumental beam variation, electronic gain variations, etc. Here, we assume that the best calibration possible is already performed. We are interested in the residual gains only, and the two-point correlation function $\xi(\tau)$ represents the two-point correlation in the residual gain. As the gain is calibrated at a given time interval, the calibration procedure is expected to reduce the time correlation in the residual gain. However, gain errors at smaller time scales as well as long-term effects over multiple days can still be present in the residual gains. For the purpose of this work, we assume that the normalized two-point correlation function $\xi(\tau)$ of the residual gain error is unity at zero delay τ and model it as

$$\xi(\tau) = \exp\left[-\frac{\tau^2}{2T_{corr}^2}\right] \tag{5.6}$$

where T_{corr} gives the correlation time of the residual gains. Note that the above model considers that the residual gain errors have only short time-scale variations, and they do not have any long-term correlation. In reality, the two-point correlation function of the residual gain error can be rather complicated. In practice, it needs to be estimated for any observation and used to calculate the effect of residual gain for the given observation.

5.2 Analytical Estimates of Bias and Variance of the Power Spectrum

This section finds an analytical estimate for the bias and variance in the power spectrum estimator for a given gain error model. Here, we restrict ourselves to a single frequency channel. The effect of frequency-dependent residual gain errors will be discussed in the next chapter. Using a numerical simulation of observed visibilities with a model of residual gain errors in Chapter 4, we have shown that the latter introduces bias in the power spectrum estimates. Here we use an improved model for the gain error and provide an analytical estimate for both bias and variance of the power spectrum in the presence of residual gain errors and noise for the power spectrum estimator discussed above. These analytical expressions are then compared with simulated observations.

5.2.1 Effect of gain errors in visibility correlation

As discussed above, correlating the observed visibilities at nearby baselines gives an unbiased estimate of the power spectrum in the presence of no residual gain errors. However, in the presence of gain errors, the estimator discussed above is biased, and the uncertainties in the estimates of the power spectrum increase. This is particularly important while observing a field that requires a high dynamic range in sensitivity. To understand the additional effect of gain errors, we discuss how we can get a pair of nearby baselines in a given uv-grid where the visibilities are measured and correlated. Note that visibility is measured by correlating the electric fields from a pair of antennas. The visibility is measured at a baseline $\vec{U}$ given by the antenna separation projected in the plane of the sky, weighted by the inverse of the observing wavelength. As the sky rotates with respect to the observer, the same pair of antennae gives rise to different measurements of the visibilities at different baselines $\vec{U}$. Hence, for a given antenna pairs A and B, at a time t, the visibility

is measured at a baseline $\vec{U}_{AB}(t)$, we write this visibility as $\tilde{V}_{AB}(t)$. We can get a pair of baselines for nearby baseline correlation in four different ways, as discussed in Chapter 4. These are:

- **Type 1** Correlation of the visibilities measured by the same antenna pair, at different times, i.e. $\langle \tilde{V}_{AB}(t)\tilde{V}^*_{AB}(t')\rangle$
- **Type 2** Correlation of the visibilities measured by antenna pairs having one antenna in common, measured at the same time, i.e. $\langle \tilde{V}_{AB}(t)\tilde{V}^*_{AC}(t)\rangle$
- **Type 3** Correlation of the visibilities measured by antenna pairs having one antenna in common measured at different times. $\langle \tilde{V}_{AB}(t)\tilde{V}^*_{AC}(\ t')\rangle$
- **Type 4** Correlation of the visibilities measured by antenna pairs having no antenna in common measured at any time. $\langle \tilde{V}_{AB}(t)\tilde{V}^*_{CD}(t')\rangle$.

Note that the noise is uncorrelated between any two measurements considered for the above cases. If we consider any uv-grid in the baseline plane in which all nearby baseline correlations are performed to estimate the power spectrum, then those baseline pairs may have a contribution from all four cases discussed here. As gain in the interferometer depends on the antenna, different types of baseline pairs contribute differently to the excess gain and uncertainties of the visibility correlations. We define the fraction of baseline pairs of type 'i' (where i can be any of 1-4 above) as $n_i(\vec{U}_g)$ in a uv-grid. Clearly, this depends on the baseline of the uv-grid $\vec{U}_g$ through the antenna configuration of the telescope and source position for observation.

5.2.2 Bias and Variance of the power spectrum

The formalism to include the effect of residual gain errors in the bias and variance of the power spectrum is rather general and can be used for any high dynamic range observations.

Here we are particularly interested in the case of observing the power spectrum of redshifted 21-cm brightness fluctuations from the EoR. Another complication in observing the redshifted 21-cm signal is the presence of emissions from the foregrounds in the observing frequency. We may write the sky visibility $\tilde{V}^S(\vec{U}_i)$ as a combination of the redshifted 21-cm signal $\tilde{V}^{HI}(\vec{U}_i)$ and the foreground $\tilde{V}^F(\vec{U}_i)$ as

$$\tilde{V}^S(\vec{U}_i) = \tilde{V}^{HI}(\vec{U}_i) + \tilde{V}^F(\vec{U}_i). \tag{5.7}$$

In the context of 21-cm emission, if $\tilde{V}^S(\vec{U}_i)$ has a contribution only from the 21-cm emission since the residual gain errors are expected to be much smaller than unity, the bias in the power spectrum is rather small and can be ignored. The effect of the residual gain errors manifests itself in the presence of a bright foreground signal. The power spectrum of the foreground is known to be six to seven orders of magnitude higher amplitude than that of the redshifted 21-cm signal (Di Matteo et al., 2002; Shaver et al., 1999). Hence, observation of the 21-cm power spectrum requires high dynamic range calibration. Here, we assume that a good estimation of the foreground signal already exists, and a foreground subtraction has been performed to extract the 21-cm signal from the observed visibilities. Further, the foreground and redshifted 21-cm signals are also assumed to have no correlation. If these visibilities are now used to estimate the 21-cm power spectrum, the estimates will have bias and increased uncertainties. The excess bias and variance in the power spectrum in the presence of the residual gain errors is a combined effect of the gain errors and foregrounds (Kumar et al., 2020). As discussed earlier, the power spectrum estimator discussed here is unbiased in the absence of residual gain errors. We define the bias in the power spectrum estimator as the difference in the power spectrum with and without residual gain errors. Ali et al. (2008); Dutta (2011) discuss the calculation of uncertainty in the power spectrum estimates by the propagation of noise in visibilities. Here, we adopt a similar method to calculate the uncertainty in the power spectrum in

the presence of residual gain errors as the variance of the visibility correlation with the propagation of errors coming through the noise and residual gains. We denote the bias in the power spectrum estimate as $\mathscr{B}_P(U)$ and its variance as $\sigma_P^2(U)$. With the assumptions described earlier, the analytical expression for the bias and variance in H I power spectrum estimates in an annulus have the following forms:

$$\begin{aligned}
\mathscr{B}_P &= [(2n_1+n_3)\chi+n_2]\,\frac{(\sigma_R^2+\sigma_I^2)}{N_d}P_F, \qquad (5.8)\\
\sigma_P^2 &= \left[\frac{P_{HI}^2}{N_G}+\frac{2\sigma_N^2 P_{HI}}{N_B N_d}+\frac{2\sigma_N^4}{N_B N_d^2}\right]+\left[\frac{4\sigma_N^2(\sigma_R^2+\sigma_I^2)P_F}{N_B N_d^2}\right]\\
&+ \left[\left[(4n_1^2+n_3^2)\chi^2+n_2^2\right]\left[3\sigma_R^4+3\sigma_I^4+2\sigma_R^2\sigma_I^2\right]+8(\sigma_R^4+\sigma_I^4)\frac{4\sigma_N^2P_F^2}{N_G N_d^2}\right]
\end{aligned}$$

Here N_d is the number of days of observation, and P_F is the power spectrum of the foreground signal. We assume that the power spectrum of the foreground is much higher than that of the redshifted 21-cm signal. In reality, there is a contribution to bias from the 21-cm signal as well; however, they are much smaller than the signal itself and hence are ignored here. The quantities N_G and N_B are the number of independent estimates of the power spectrum and the total number of visibility correlations in a baseline annulus. We assume here that the noise and residual gain errors are not correlated between the observations done on different days; N_d is the number of days of observation. Note that bias and variance change with baseline, and apart from σ_N, σ_R, and σ_I, all the other factors in the expressions for bias and variance are baseline-dependent. The term $\frac{P_{HI}^2}{N_G}$ is the contribution from the sample variance and decreases with the baseline. In all our investigations presented here, this term is negligible. A detailed calculation of the analytical expressions of bias and variance, along with the assumptions, is presented in Appendix B.

For convenience, we define

$$\begin{aligned}
\text{Term 1} &= \left[\frac{P_{HI}^2}{N_G} + \frac{2\sigma_N^2 P_{HI}}{N_B N_d} + \frac{2\sigma_N^4}{N_B N_d^2}\right] \\
\text{Term 2} &= \left[\frac{4\sigma_N^2(\sigma_R^2+\sigma_I^2)P_F}{N_B N_d^2}\right] \\
\text{Term 3} &= \left[\left[(4n_1^2+n_3^2)\chi^2+n_2^2\right]\left[3\sigma_R^4+3\sigma_I^4+2\sigma_R^2\sigma_I^2\right]+8(\sigma_R^4+\sigma_I^4)\frac{4\sigma_N^2 P_F^2}{N_G N_d^2}\right]
\end{aligned} \tag{5.9}$$

As expected, the power spectrum estimator is unbiased in the absence of gain errors. Hence, the 'Term 1' in variance is independent of the gain errors. The 'Term 2' and 'Term 3' represent the contribution in the variance of the power spectrum arising because of the presence of residual gain errors and depend on residual gain errors through both (σ_R, σ_I) and χ. The function χ is non zero, if the correlation time of the residual gain errors T_{corr} are larger than the integration time $\Delta\tau$ and is given by

$$\chi(U) = \frac{1}{T_D^2}\int_{\Delta\tau}^{T_D}(T_D-\tau)\xi(\tau)d\tau. \tag{5.10}$$

Here $T_D = \frac{\Delta U \times T_{24}}{2\pi U}$ is the time taken by baseline track of an antenna pair to cross a uv-grid of size ΔU at baseline U. T_{24} corresponds to one sidereal day. The function $\chi(U)$ gives the integrated effect of the time-correlated residual gain errors over the uv-grids. If the gain errors do not have any time correlation, $\chi(U)$ is zero, and the contribution to bias and variance originates from Σ_R and Σ_I only. In the presence of time-correlated residual gain errors, the function $\chi(U)$ needs to be calculated additionally.

As time progresses, a pair of antennae defines different baseline vectors and traces an elliptical track in the baseline plane. The contribution from the time-correlated gain errors also comes through the baseline pairs of type 1 and 3. The baseline pair of type 4 does not contribute to the bias and variance. This is expected as this type has four different antennas, and we have assumed that the residual gain errors in the different antennas are uncorrelated.

We observe that if the gain errors are not correlated in time, that is $T_{corr} = 0$, the residual gain errors still introduce bias and excess variance in the power spectrum estimates. We have neglected terms higher than the fourth power in the standard deviation of residual gain errors in the calculation shown here.

Note that we use a foreground subtraction approach here (Bowman et al., 2009; Choudhuri et al., 2017b; Morales et al., 2006), where the power spectrum is calculated by correlating the visibilities in the same observed frequency channel. Though the foreground avoidance method is expected to reduce the effect of foreground drastically from the visibility correlation (Datta et al., 2010; Morales et al., 2012; Vedantham et al., 2012), it is important to observe that H I signal correlation at different frequency channels also reduce the H I signal (Bharadwaj and Ali, 2005; Bharadwaj and Pandey, 2003). Furthermore, a residual bandpass component, like the residual time-dependent gain considered here, will also leak the foreground to the outer part of the wedge. Due to the bandpass calibration uncertainties, the correlated sky signal residuals will remain in the data, which will lead to power in the 2-D power spectrum contaminating the EoR window (Barry et al., 2016; Morales et al., 2012; Patil et al., 2016; Trott and Wayth, 2016). These effects of residual frequency-dependent gains will be presented in the next chapter of this thesis.

5.3 Comparing analytical expression of bias and variance with simulation

Here we study the effect of residual gain errors in estimating the redshifted 21-cm power spectrum in the presence of bright foreground. As has been shown analytically, residual gain errors introduce a bias and enhance the variance of the power spectrum. The bias and variance of the power spectrum depend on the gain error model, baseline configuration, and foreground model. This section compares the analytical results against simulated

observations with a given gain error and foreground model. We use the Upgraded Giant

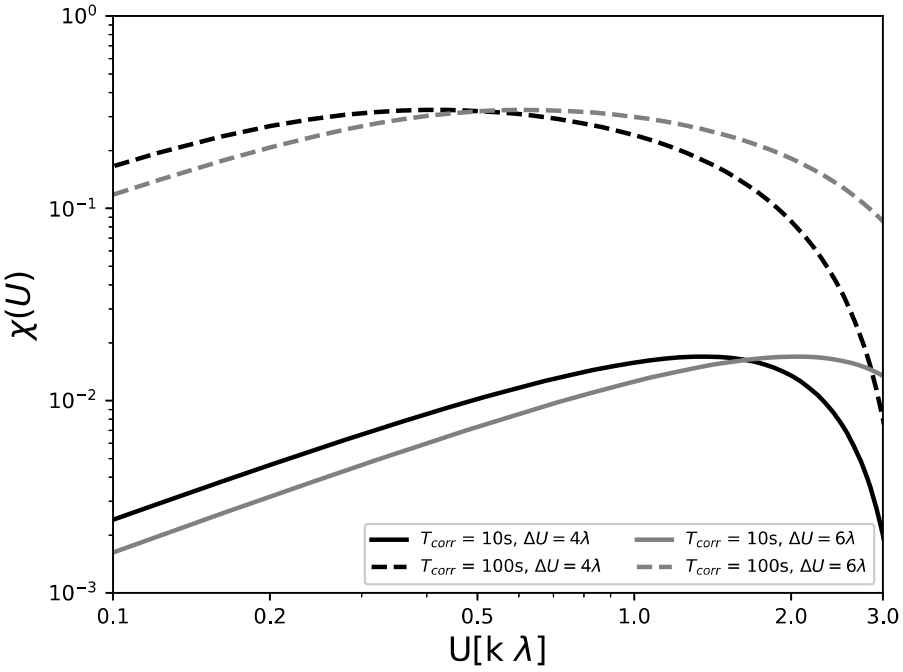

Fig. 5.1 Variation of χ with baseline U for different correlation times T_{corr} and uv-grid size ΔU for an integration time of 16 seconds.

Metrewave Radio Telescope (uGMRT) [‡] baseline configuration for simulating the effect of gain errors. The uGMRT has thirty fully steerable 45 meter diameter parabolic dishes spread over a region with a maximum antenna separation of 25 kilometers. We set up the observation at a central frequency of 150 MHz, where the telescope gives a circular field of view with a radius of $\theta_0 = 186^{'}$ and a maximum baseline of 12.5 kλ. As we are interested in the effect of gain in a single frequency channel here, we choose a channel width of 62.5 kHz. Given that the system temperature at this frequency is dominated by its contribution from the sky, the above configuration gives $\sigma_N = 1.36$ Jy of noise per visibility for 15 sec integration time.

[‡]The upgraded GMRT: opening new windows on the radio Universe (Gupta et al., 2017)

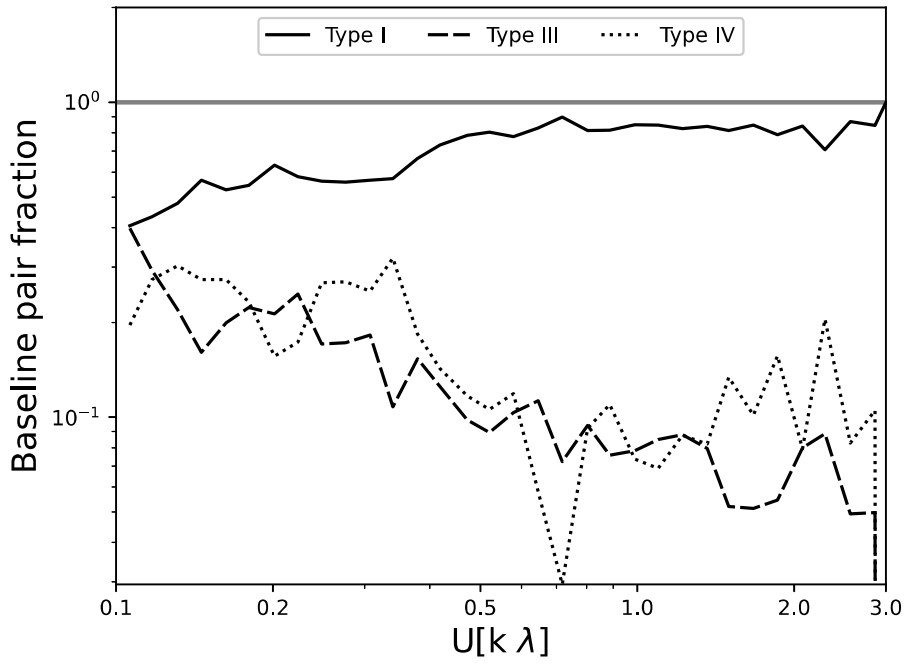

Fig. 5.2 Variation of baseline pair fractions with baseline U for GMRT, 8 hours of observation. Integration time is 16 sec and uv-grid size is 0.004 $k\lambda$. The fraction of baseline pairs of type II is zero for the above-used parameters for GMRT.

The major modification in the bias and variance of the power spectrum arises from the bright foreground. Here we use a point source foreground model based on the differential source count at 150 MHz estimated in Intema et al. (2017). We use this differential source count to generate a point source sky model. The previous chapter describes the methodology followed to generate the point source sky model, and we follow a similar procedure here. To consider the effect of sample variance, we generate 128 realizations of the point source sky models. All the models have 7250 sources with flux density ranging between 300 mJy to 1 Jy over a radius of $200^{'}$. The redshifted 21-cm power spectrum at 150 MHz is $10^6 - 10^7$ times smaller than the foreground and provides a minimal effect on the bias and variance of its power spectrum in the presence of residual gain errors. We do not include the 21-cm signal in our simulation. To consider a specific baseline distribution,

we choose the declination of the center of our simulated point source field at $+30^\circ$ and a total observation time of eight hours symmetrically distributed from the transit time of the source. This configuration is also used to estimate the baseline pair fractions for the analytical calculation of the bias and variance of the power spectrum. Figure 5.1 shows the variation of χ as a function of baseline for different combinations of T_{corr} and uv-grid size ΔU. For all choices of ΔU and T_{corr}, the effect of χ is less at shorter baselines and is effectively negligible at longer baselines. A larger correlation time increases the amplitude of χ and hence its contribution to the bias and variance of the power spectrum. Since the limits in the integration for χ depend on the uv-grid size, we also see that a larger uv-grid size keeps the value of χ at a significant level for a longer baseline value. This suggests a gain calibration with a lower correlation time for residual gain, and a smaller uv-grid size is preferred to reduce the bias and variance of the power spectrum. We choose a uv-grid size $\Delta U = 4\ \lambda$ for further calculations. This is smaller than $1/(\pi\theta_0) = 6\ \lambda$ and large enough to accommodate enough baseline pairs in most of the uv-grids. Figure 5.2 show the variation of the baseline pair fractions as a function of U. We observe that the uGMRT configuration provides mainly the baseline pairs of type I for visibility correlation, whereas the baseline pair of type II is completely absent. As we will see, the baseline pair fractions have a significant role in deciding the strength of the bias and excess variance in the power spectrum. We also note that the baseline pair fractions are expected to be significantly different for different telescopes.

Bharadwaj and Ali (2005) has estimated the expected redshifted 21-cm power spectrum at different observing frequencies. They find that at 150 MHz, the power spectrum remains almost constant to about 0.5 kλ, and its amplitude reduces drastically beyond 2 kλ. Hence, we show the baseline pair fractions up to 3 kλ only. We observe that $n_2 \sim 0$ and baseline pair fraction of type 1 dominates for all baselines. The gain error model we discussed earlier can be expressed in terms of three parameters σ_R, σ_I and T_{corr}. Given the baseline

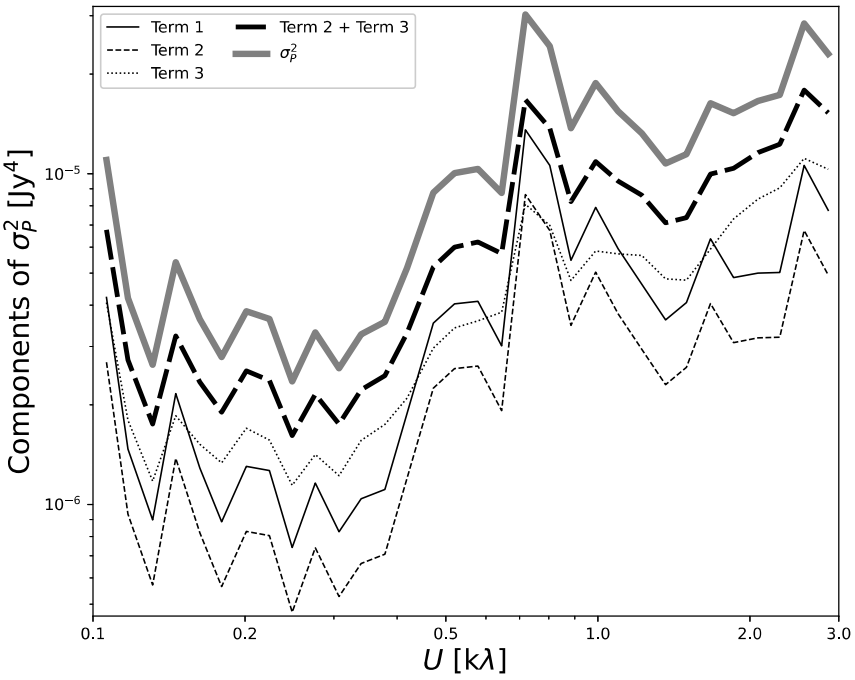

Fig. 5.3 Comparison of contribution from different terms in the expression for the variance of the power spectrum σ_P^2. The result shown here is for 8 hours of the uGMRT observation with an integration time of 16 sec and bandwidth of 256 kHz. We have chosen 5% gain error in both real and imaginary parts of the visibilities and $T_{corr} = 16$ seconds.

configuration of the observation, the uv-grid size chosen, and the integration time, we simulate the visibilities with different values of the parameters σ_R, σ_I and T_{corr} for each of the point source sky models for 8 hours of total observation time. We also estimate the ideal visibilities expected from each sky model while no gain errors or measurement noise is present. The residual visibilities are calculated by subtracting the ideal visibilities from the simulated ones [§]. We then estimate the power spectra of the residual visibilities for all 128 sky models. The mean of the power spectra from 128 realizations provides an estimate of the bias in the power spectrum arising from residual gain errors. The variance of the

[§]Note that here ideal visibilities represent a known foreground sky model. In practice, such foreground models are derived from observations with their associated uncertainties. Hence, the results presented here can be considered the best-case scenario when the foreground estimation is robust.

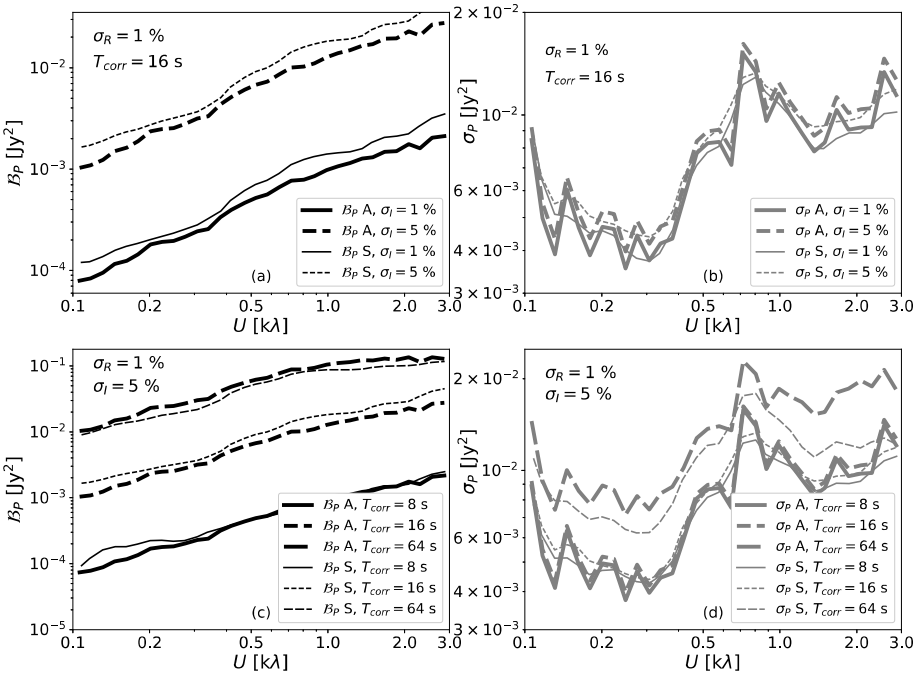

Fig. 5.4 We compare the analytical estimates of $\mathscr{B}_P$ (thick black) and σ_P (thick grey) with their estimate from simulation (thin black and thin grey respectively for $\mathscr{B}_P$ and σ_P). On the left side, we show the comparison plots for $\mathscr{B}_P$, and the comparison plots for σ_P are shown on the right side. The plots are shown for eight hours of observing time and a bandwidth of 64 kHz. In the top panel we keep $\sigma_R = 1$ % and $T_{corr} = 16$ sec and show $\mathscr{B}_P$ in (a) and σ_P in (b), for different values of σ_I. In the bottom panel we fix $\sigma_R = 1$ % and $\sigma_I = 5$ % and show the bias $\mathscr{B}_P$ in (c) and σ_P in (d), for $T_{corr} = 8, 16, 64$ seconds.

power spectra from 128 realizations gives an estimate of the excess variance arising due to residual gain errors. These are then compared with analytical calculations done with the same gain error models, baseline pair fractions of the observation, and measurement noise.

We show the relative contributions of different terms in the expression of σ_P^2 in figure 5.3. For the set of parameters used here, the contribution from the gain error (Term 3) dominates over the system noise (Term 1). However, this behavior changes for different choices of the gain parameters and will be discussed shortly. Interestingly for the particular case shown here, the contribution in the uncertainty from different terms has similar

baseline dependence. This indicates that the baseline dependence is mostly a result of the variation of total baseline pairs present in an annulus (N_B) as a function of baseline and depends less on the other baseline-dependent factors.

Figure 5.4 compares the analytical results with that of the simulation of bias and variance in the power spectrum estimator for different gain model parameters. The bias $\mathscr{B}_P$ is plotted with the black lines in the left panel, and the grey lines show the standard deviation σ_P in the right panel as a function of the baseline. The thick curves are for analytical estimates and are denoted in the legend with 'A'. As denoted as 'S' in the legend, the thin curves show the corresponding results with simulations. In top panel of the figure 5.4, we keep $\sigma_R = 1$ % and $T_{corr} = 16$ sec, same as the integration time for this observation. The solid and dashed lines show for $\sigma_I = 1.0$ % and 5 % respectively. In plot (a) we show the bias $\mathscr{B}_P$ and in (b) we show the standard deviation σ_P. We observe that $\mathscr{B}_P$ is significantly lower than σ_P for $\sigma_I = 1.0$ % and it is comparable in case of $\sigma_I = 5.0$ %. An increase in σ_I also increases the bias. For these gain error parameters, the variance is dominated by the system noise and hence does not vary much with gain error models. A $\sigma_R = \sigma_I = 1$ % corresponds to 1.0 % error in estimation of the amplitude and 0.6° error in estimation of the phase of visibilities. Similarly for $\sigma_R = 1$ %, $\sigma_I = 5$ %, these numbers will corresponds to 1.0 % error in estimation of the amplitude and 3° error in estimation of the phase. In the bottom panel of figure 5.4, we show the variation of $\mathscr{B}_P$ in (c) and σ_P in (d) for different values of T_{corr} while σ_R and σ_I are kept at 1 % and 5 % respectively. We see that both $\mathscr{B}_P$ and σ_P increases with increase in T_{corr}. For these gain model parameters change in $\mathscr{B}_P$ is more than σ_P for different T_{corr} and $\mathscr{B}_P$ exceeds the σ_P for $T_{corr} = 64$ seconds. If we keep σ_R and σ_I at the same value, we shall refer to it as $\sigma_g = \sigma_R = \sigma_I$ henceforth.

Figure 5.4 demonstrates that the variance estimates from the simulation match with their analytical expression quite well. The analytical expression of the bias follows the estimates

from the simulation with a slight offset for some of the gain model parameters. However, these departures are relatively small. We conclude that the analytical expression for the bias and variance of the power spectrum we have presented here is in good agreement with the results from the simulation. This allows us to assess the effect of residual gain errors for different gain error models without referring to simulated observations, reducing the computation time significantly.

5.4 Results: Different effects of gain errors

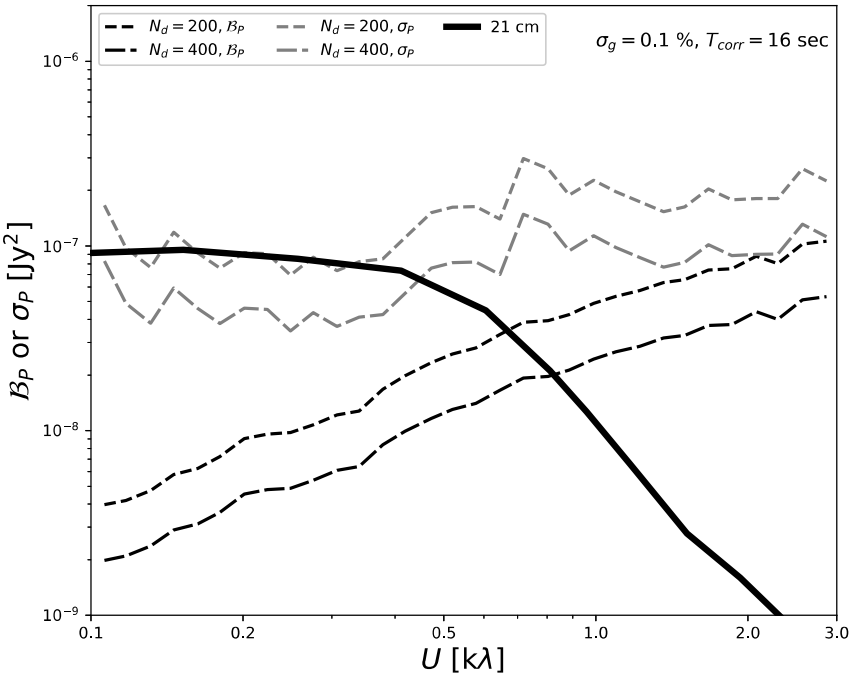

Fig. 5.5 Variation of $\mathscr{B}_P$ (thin black) and σ_P (thin grey) with baseline is shown for 100 and 400 days of observing time. Here, we consider a bandwidth of 16 MHz, and a correlation time of $T_{corr} = 16$ seconds. Both the quantities σ_R and σ_I are set to $\sigma_R = \sigma_I = \sigma_g$. The thick black line corresponds to the expected EoR power spectrum (Bharadwaj and Ali, 2005).

In the previous chapter, we use a slightly different model for the gain error, where the normalized two-point correlation function of the residual gains is assumed to be unity at zero delay and falls smoothly as a power-law at the larger delay. There we estimate the bias in the power spectrum using simulated observations. The gain error model discussed in this work is distinct from the one described in the previous chapter in the sense that it uses an exponential function for the two-point correlation of the residual gains. However, they both assume the two-point correlation function of the residual gains to be unity at zero delay and zero at the large delay. In this work, we establish an analytical expression that can be used to estimate the effect of gain error in the power spectrum for the gain error model discussed in section 5.1. In this section, we use the analytical expression for the bias and variance of the power spectrum to investigate the various effects of gain errors. It is important to note that the estimates of the bias and variance of the power spectrum presented in this work are based on a simplified model for gain error and are by no means complete. We expect to have different effects, sometimes larger than what is discussed here, arising from various other sources like long-time correlation, non-Gaussian effects and frequency correlation in gain errors, an inaccurate estimate of the sky model, foreground, etc. Hence, the numbers presented here should be taken only in the context and model of the gain errors discussed here.

Assuming that the gain errors are not correlated in frequency and across different days of observation, we first investigate the time required to detect the EoR 21-cm signal at 150 MHz in the presence of residual gain errors. Here we have considered an observation bandwidth of $\Delta\nu = 16$ MHz with $\Delta\tau = 16$ sec of time integration per visibility. The bandwidth directly affects the system noise of the interferometer, whereas the integration time affects the system noise as well as the total number of baseline pairs in a given uv-grid where the power spectrum is estimated. For most of the analysis presented henceforth, we use the above values of $\Delta\nu$ and $\Delta\tau$. We shall discuss the effect of the integration time later.

We observed in figure 5.4 earlier that the gain error increases with both σ_R and σ_I as well as T_{corr}. Here we choose a relatively moderate value for $\sigma_g = 0.1$ % and correlation time $T_{corr} = 16$ seconds. Using the analytical expression given in section 5.2.2. we calculate $\mathscr{B}_P$ and σ_P for different number of days of observations $N_d = 200, 400$ and the result is shown in fig 5.5. With the combinations of σ_g and T_{corr} discussed here, we observe that $\mathscr{B}_P$ is consistently less compared to σ_P at all baselines. Hence, for the parameter values given here, detection of the redshifted 21-cm signal would depend on the modified σ_P. The thick black curve in this figure shows the expected 21-cm power spectrum (adapted from Bharadwaj and Ali, 2005). The 21-cm power spectrum at this observing frequency remains almost constant up to a baseline of ~ 0.4 kλ and falls rapidly at higher baselines. If the gain error model presented here were the only source of power spectrum estimation error, we see that for observation of 200 days $\sigma_P \sim P_{HI}$ for $U < 0.4$ kλ. As $\sigma_P \sim 1/N_d$, we expect a $3-\sigma$ detection of the power spectrum for 600 days of observation. Note that, as discussed earlier, in practice, there are expected to be more systematic effects other than what is discussed here that may require more stringent observational requirements. If excellent bandpass calibration is achieved, the effect of time-correlated gain error could become a dominant calibration error mechanism. Accuracy of the foreground model, efficacy of foreground subtraction procedure, unmitigated residual RFI, polarisation leakage, and non-Gaussianity in noise, amongst other things that can also increase the uncertainty in power spectrum estimate. For the compact source foreground model considered here, we observe that the baselines > 1 Kλ are relatively more affected by the residual gain errors. This is partly because the $\mathscr{B}_P$ is systematically higher at longer baselines. However, the main reason may be that the amplitude of the expected redshifted 21-cm power spectrum reduces drastically beyond 0.4 kλ. In the rest of the discussion, we investigate the effect of residual gain errors at the baseline of 0.3 kλ. We also consider $\Delta\nu = 16$ MHz, $\Delta\tau = 16$ sec, and a total of 400 days of observation in the subsequent cases discussed here.

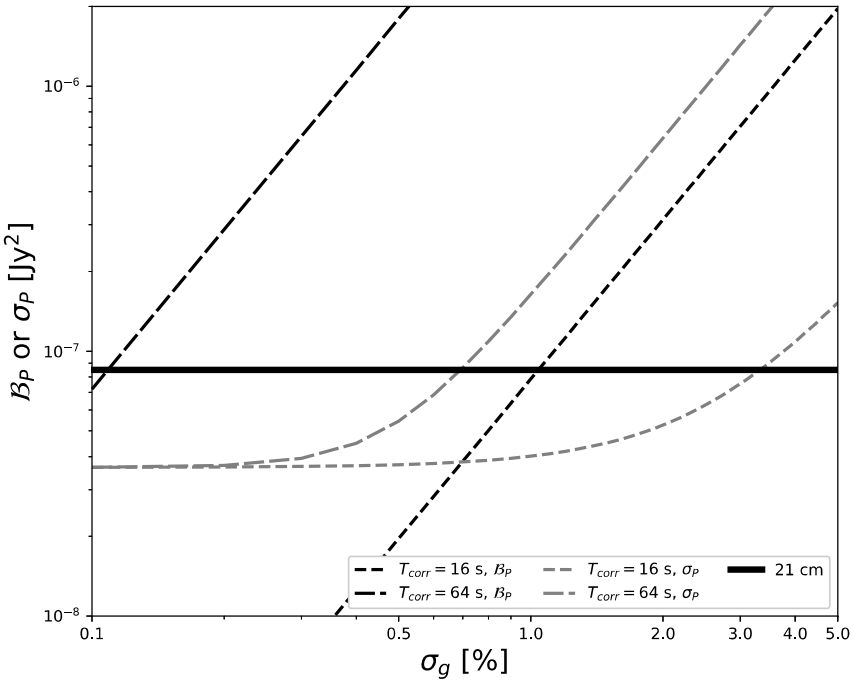

Fig. 5.6 Variation of $\mathscr{B}_P$ (thin black) and σ_P (thin grey) with $\sigma_R = \sigma_I = \sigma_g$ for correlation time $T_{corr} = 16, 64$ seconds. Here, we consider a bandwidth of 16 MHz, and an observation time of 400 days. The plots are made at a baseline of 300 λ. The thick black line corresponds to the expected EoR power spectrum (Bharadwaj and Ali, 2005)

Figure 5.6 show the variation of $\mathscr{B}_P$ (thin black lines) and σ_P (thin grey lines) with σ_g at a baseline of 0.3 kλ. The thick horizontal black line corresponds to the expected EoR power spectrum at this baseline. The dashed curves show results with $T_{corr} = 16$ sec, whereas the dot-dashed curves show results with $T_{corr} = 64$ seconds. In eqn 5.8, the term $\sigma_R^2 + \sigma_I^2 = 2\sigma_g^2$ and hence it is expected that the bias increases with the value of σ_g quadratically. This can be clearly seen in the figure. For small values of σ_g, the third term in the expression of σ_P in eqn 5.9 dominates and it remains constant at well below the EoR power spectrum. We see that for $\sigma_g = 0.5$ % or higher the effect of σ_g is more pronounced. We also observe that at lower values of σ_g, σ_P has a greater effect than the bias, as the gain error increases though, the power spectrum estimates become significantly biased.

We observe that for cases with lower T_{corr}, i.e, for $T_{corr} = 16$ sec, the contribution from $\chi(U)$ is rather small and both $\mathscr{B}_P$ and σ_P are lower.

We investigate the effect of the correlation time T_{corr} in figure 5.7, where we keep σ_g fixed and vary T_{corr} from 4 to 128 seconds. Note that, the integration time is fixed at 16 seconds for all these cases. The effect of T_{corr} comes through the function χ in both $\mathscr{B}_P$ and σ_P. The terms in the expression for $\mathscr{B}_P$ and σ_P involving χ depend on the baseline pair fraction of type 1 and 3. Hence, for an interferometer baseline configuration with these baseline pair types relatively low, T_{corr} would have a lesser effect. We observe that for small values of σ_g, σ_P is rather small, below the expected EoR signal, and almost remains independent of T_{corr}. When $\sigma_g = 1$ % is considered, σ_P is still small at lower T_{corr}, but then increases drastically beyond 32 seconds. The bias in the power spectra, on the other hand, is rather large and well above the EoR signal for $T_{corr} < \Delta\tau$ with $\sigma_g = 1$ %. For both the cases of σ_g, there is a transition point for T_{corr} where $\mathscr{B}_P$ becomes dominant over σ_P. In interferometric calibration, we estimate the gain as a function of time and try to reduce its effect on the observed data. Hence, the time correlation in the residual gain errors is not expected to be present at the time interval the gains are estimated. As each visibility measurement is integrated over the time $\Delta\tau$, the time variation can be estimated at best to a time scale of $\Delta\tau$. Hence, any time correlation in the residual gain errors can be at best reduced for $T_{corr} > \Delta\tau$. The maximum integration time for any interferometer is limited by the time-smearing effect that arises from its largest baselines owing to integration time. For the GMRT, the maximum integration time that can be safely taken is $\Delta\tau = 16$ seconds. As one lowers $\Delta\tau$, there are two competing effects. On the one hand, the noise in each visibility increases (see eqn 5.2). At the same time, the number of baseline pairs in a given uv-grid N_B also increases. Hence, getting a reliable calibration solution for an arbitrarily small integration time is difficult. This suggests that there can be an optimum integration time choice possible for a given observation and other parameters. We show

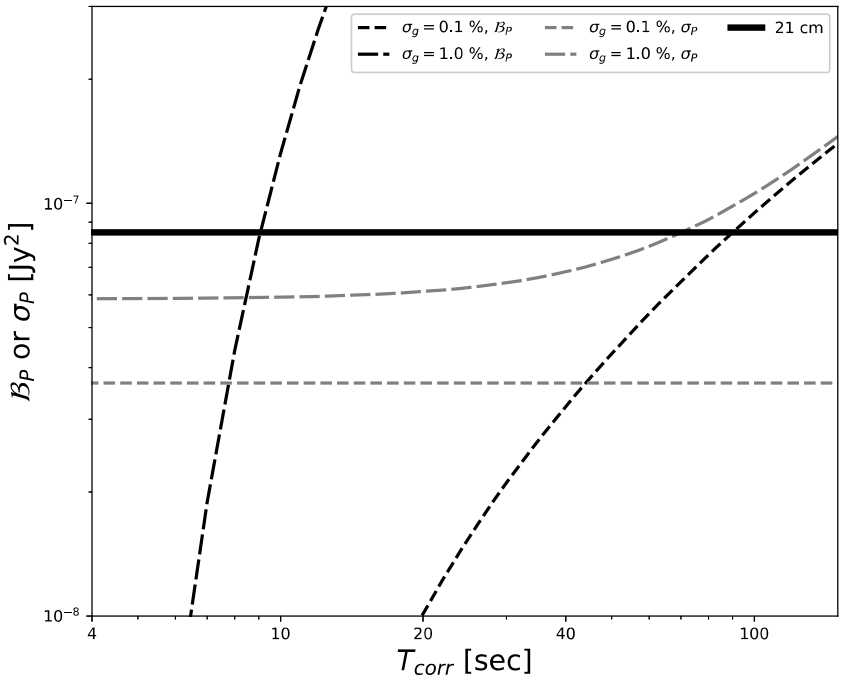

Fig. 5.7 Variation of $\mathscr{B}_P$ (thin black) and σ_P (thin grey) against different correlation time with $\sigma_R = \sigma_I = \sigma_g = 0.1, 1.0$ %. Here, we consider a bandwidth of 16 MHz and an observation time of 400 days. The plots are made at a baseline of 300 λ. The thick black line corresponds to the expected EoR power spectrum (Bharadwaj and Ali, 2005).

the variation of $\mathscr{B}_P$ (thin black) and σ_P (thin grey) with $\Delta\tau$ in the figure 5.8 for two values of $\sigma_g = 0.1, 1.0$ %. We observe that the bias increases monotonically as integration time increases irrespective of the value of σ_g; though, for lower σ_g, the bias is negligible. The value of σ_P is rather high for lower integration times and decreases with the increase of $\Delta\tau$. This is because at lower values of $\Delta\tau$ the contribution from the last term in the expression of σ_P dominates through the foreground factor. The third term becomes important at larger $\Delta\tau$ through σ_N/N_B. We see that for $\sigma_g = 1$ %, this eventually makes σ_P fall below $\mathscr{B}_P$.

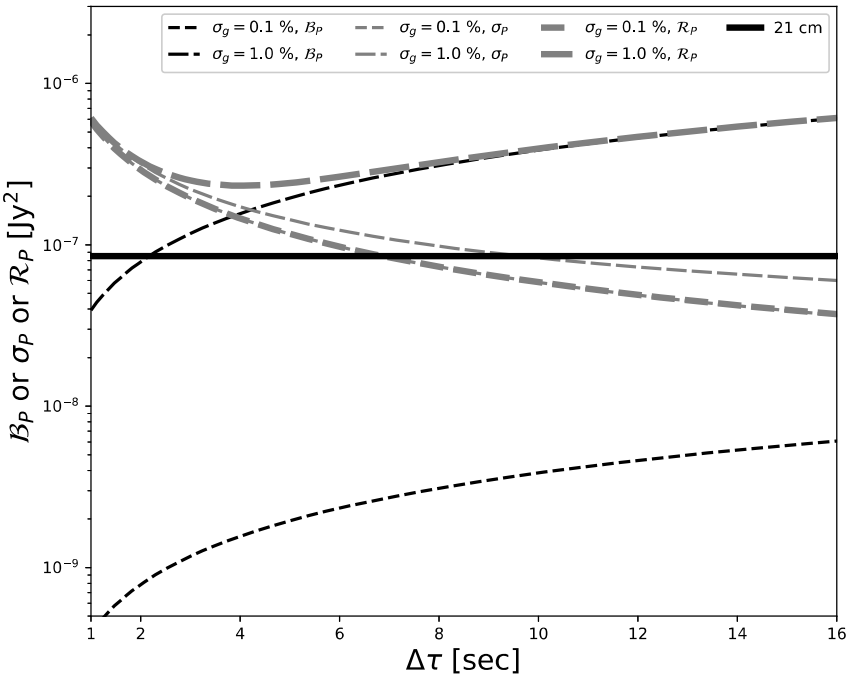

Fig. 5.8 Variation of $\mathscr{B}_P$ (thin black) and σ_P (thin grey) against different integration time $\Delta\tau$ with $\sigma_g = 0.1, 1.0$ %. Here, we consider a bandwidth of 16 MHz, and an observation time of 400 days. The plots are made at a baseline of 300 λ. The correlation time for the gain errors are kept the same as $\Delta\tau$. The thick black line corresponds to the expected EoR power spectrum (Bharadwaj and Ali, 2005). The thick grey lines show the values of Risk $\mathscr{R}_P$ as defined in the eqn 5.11

.

We define the risk [¶] as

$$\mathscr{R}_P^2 = \mathscr{B}_P^2 + \sigma_P^2, \tag{5.11}$$

The risk for the two cases shown here is plotted with thick grey lines. As the bias for the case with $\sigma_g = 0.1$ % is significantly low, the risk mostly follow its σ_P. On the other hand, for the case with $\sigma_g = 1.0$ %, we see that risk is at its lowest for an integration time of 4 seconds. This demonstrates that for such high dynamic range observations, one needs to

[¶]Note that this is different from the usual definition of risk. Here we use this to keep it of the same dimension of $\mathscr{B}_P$ (thin black) and σ_P.

assess the gain properties of the telescope and can optimally choose the integration time for observation. Note that it is always possible to use the lowest integration time; however, as this exercise demonstrates, one needs to integrate the visibilities to an optimal time prior to using visibility correlation.

Regular interferometric calibration uses observation of calibrator sources to assess the large time-scale variation of the gain. However, one uses the self-calibration procedure to mitigate the time dependence of the gain at a few tens of seconds time scale. Here one may reduce the time interval at which the gain solution is attempted and get a gain solution at a smaller time scale. This is expected to reduce the correlation time of the residual gain errors. However, estimating gain solutions at a higher time resolution reduces the number of independent measurements used to estimate the solution increasing the calibration uncertainty. In addition to the sky model, in self-calibration, the amplitude and phase closure properties are used (Thompson et al., 1986) to constrain the gain solutions of the antenna. Hence, given the telescope SEFD, the integration time of observation $\Delta\tau$, the amplitude of the signal used for calibration A_0, the time cadence at which the gains are estimated T_{sol} and the number of antenna N available to impose the closure properties in phase and amplitude, in the ideal case the variance of the real and imaginary parts of the residual gain errors differ and can be written as $\sigma_I = \sigma_g, \sigma_R = \eta\ \sigma_g$, where

$$\sigma_g^2 = \frac{2\sigma_N^2/A_0^2}{(N-1)(N-2)T_{sol}/\Delta\tau}, \tag{5.12}$$

and $\eta^2 = 3/(N-3)$. In the best possible case, the gain solutions can be obtained at the time interval of the integration, and any time correlation in the residual gain would have a lower correlation time, that is $T_{corr} = T_{sol} = \Delta\tau$. Considering a value of A_0^2 equal to the amplitude of the foreground power spectrum, the typical value of $\sigma_g \sim 0.5$ % for 16 seconds of integration time and 62.5 kHz channel width with the uGMRT. As η is

small, the main contribution to the bias and variance of the power spectrum arises from the imaginary part of the gain errors.

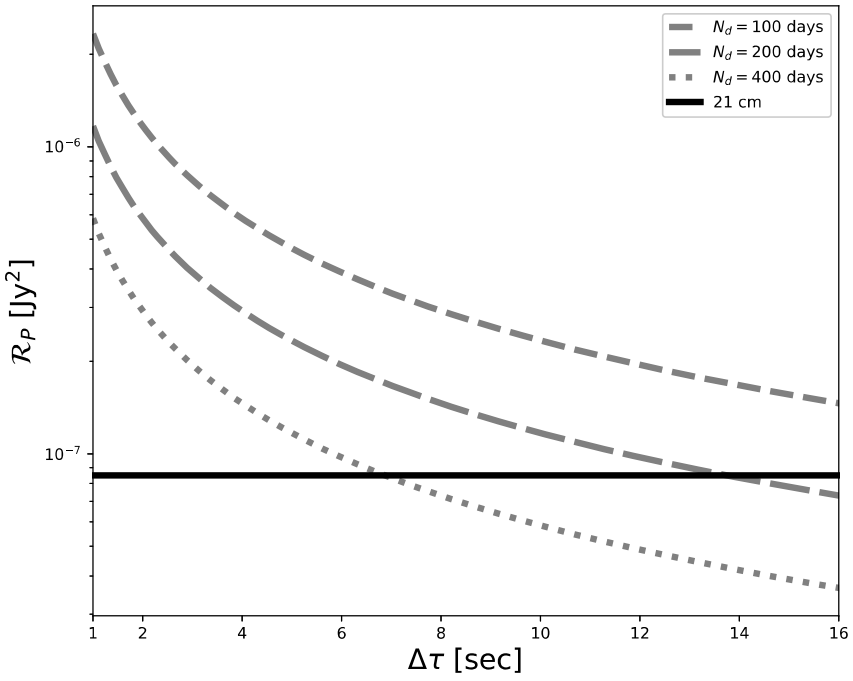

Fig. 5.9 Variation of $\mathscr{R}_P$ against different integration time $\Delta\tau$ for the best possible case with the uGMRT at 150 MHz. Here, we consider a bandwidth of 16 MHz, and observation times of 100, 200, and 400 days. The plots are made at a baseline of 300 λ. The thick black line corresponds to the expected EoR power spectrum (Bharadwaj and Ali, 2005).

Figure 5.9 show the estimates of the risk for three different total observation days with 8 hours of observation time per day for the best calibration possible with the uGMRT. We see here that the risk monotonically decreases, and the best choice is the maximum integration time allowed in the uGMRT that avoids time smearing. As the expression in eqn 5.12 suggests, the risk is expected to be less for an interferometer with more antenna and hence more baselines available for estimation of the gains. For two interferometers with the same sensitivity, the one with a larger number of antennas would have a lesser effect from the residual gain errors.

5.5 Discussion and Conclusion

The presence of bright foreground at the observing frequencies of redshifted 21-cm radiation makes detection of the cosmological H I signal more challenging. Calibration error couples with the bright foreground signal and limits the possibility of the 21-cm signal detection. In this work, we addressed the issue of estimating the redshifted 21-cm power spectrum in the presence of bright foreground and residual gain errors from calibration. The main points of the chapter are as follows:

- Using a model for the gain errors in radio interferometric observation, we derive analytic expressions for bias and variance of the power spectrum by propagating the uncertainties in visibilities from thermal noise and gain errors. This analytical expression of bias and variance is then tested against simulated observations from the GMRT, where we see a fairly good agreement between the analytical and simulation results.

- We find that the bias in the power spectrum strongly depends on both the variance of the gain errors and the correlation time, whereas the variance in the power spectrum is more sensitive to the variance in the gain errors. Also, the bias and variance depend on the foreground and baseline configuration of the telescope.

- We find that for the uGMRT, even with variance in the gain error as low as 1 %, the bias in the power spectrum exceeds σ_P for a reasonably low correlation time of the gain error. This suggests that it is important to assess the bias in the 21-cm power spectrum estimation in the presence of bright foreground, failing which a biased estimate can confuse the scientific interpretation of the signal.

- The properties of noise in individual visibilities, as well as the correlation time of gain errors, are expected to be affected by the integration time for each visibility in an observation. We find that, for a moderately low variance in gain errors, the

risk in such an observation can be minimized by choosing a moderate value for the integration time, hence increasing the possibility of an unbiased detection.

- The presented analytical formula here provides an efficient way of estimating the bias and variance of the power spectrum without performing the full simulation, hence reducing the expensive computational load enormously.

In this work, we do not consider the effect of frequency correlation in gain error, and all our estimations are done for correlating visibilities in the same frequency channel. Furthermore, this work also uses the foreground subtraction technique, where we expect to have accurate knowledge of the foreground emissions (Ghosh et al., 2012; Jelić et al., 2008). An alternative method, more regularly exercised in literature, is foreground avoidance. It has been established that the foregrounds to the redshifted 21-cm emissions remain correlated across relatively larger bandwidth (Ali et al., 2008; Chakraborty et al., 2019b; Jelić et al., 2008; Platania et al., 1998; Santos et al., 2005), whereas the H I signal decorrelates faster (Bharadwaj and Ali, 2005; Bharadwaj and Pandey, 2003). As a result, when the power spectrum is observed as a function of $(k_{\parallel}, k_{\perp})$, the foreground emission remains concentrated near the low $k_{\parallel}$, inside the 'wedge' (Datta et al., 2010; Morales et al., 2012; Vedantham et al., 2012). Note that the smaller frequency separation in the multi-frequency angular power spectrum contributes to larger $k_{\parallel}$ modes of the power spectrum. Hence, the effect of frequency-independent residual gain we see here at zero frequency separation may contribute to bias in the power spectrum beyond the wedge. Moreover, the antenna-based gains are functions of both time and frequency; the residual gain is expected to have correlated frequency dependence. Such frequency-correlated calibration errors couple the foreground power beyond the foreground wedge into the EoR window region of the 2-D power spectrum space (Barry et al., 2016; Byrne et al., 2019; Ewall-Wice et al., 2017; Pal et al., 2021). Here, we also consider that the gain errors arising from the different antennae are uncorrelated. Though this is a fairly good assumption for

the gain arising from electronics in the antenna system itself, the ionospheric effects may introduce correlated gains across the antenna. Furthermore, as the calibration procedure uses baseline-dependent gains to solve for the antenna-dependent gains, calibration errors can lead to correlated residual gain errors across the antenna. Moreover, asymmetry in the telescope aperture, mechanical fatigue of telescope structure, etc., can lead to parts of the gain errors correlated across different antennae and even across different days of observations.

Even though the demonstrations here are done with the uGMRT as a model for the interferometer, a similar analysis can be carried out for any telescope of concern, and a prior assessment of the effect of the gain errors can be made using the analytical expression presented here with minimum computation cost. Furthermore, this work emphasizes the importance of estimating and establishing the gain statistics for a given interferometer. Although we use a simple model for the residual gain error here, the calculations that lead to the analytical expression can be readily expanded for a more complicated gain error model.

****